Green Chemistry

PAPER

View Article Online
View Journal | View Issue

Cite this: *Green Chem.*, 2025, **27**, 12659

Electrochemically relevant physical–chemical properties of tetraalkylammonium salts solutions in the renewable solvent dihydrolevoglucosenone (Cyrene®); electrochemical behaviour of some representative organic molecules

José M. Ramos-Villaseñor, [a,b] Jessica Sotelo-Gil, [b] Maricarmen P. Flores-Morales, [b] Ruben Vasquez-Medrano[c] and Bernardo A. Frontana-Uribe *[a,b]

Received 1st July 2025,
Accepted 15th August 2025

DOI: 10.1039/d5gc03356j

rsc.li/greenchem

Currently, organic electrosynthesis (OES) represents an environmentally friendly methodology that avoids the use of toxic reagents and the generation of chemical waste during the synthesis of a wide variety of organic compounds. However, the continued use of harmful or toxic organic solvents remains a significant environmental concern. Therefore, to achieve the ecological goal of reducing the amount of organic solvents or replacing them, it is essential to investigate the electrochemistry of more environmentally friendly solvents derived from renewable sources. Dihydrolevoglucosenone (DLG or Cyrene™) is a biodegradable, bio-renewable solvent produced from cellulose mass. Its dielectric constant is comparable to that of DMF, NMP, and DMAc, which makes it a suitable candidate for applications in organic electrochemistry. Consequently, this work investigates the conductivity, viscosity behaviour, and IR spectroscopy of tetraalkylammonium salt solutions in DLG, which are commonly used as supporting electrolytes in OES. Additionally, the study of the electrochemical behaviour of representative molecules (ferrocene, phenol, EDOT, indole, morpholine, phthalimide, and nitro derivatives) demonstrates the feasibility of utilising this renewable solvent in electrochemical applications.

Green foundation

1. This study assesses the electrochemically relevant physicochemical properties of electrolytic solutions in the bio-renewable solvent dihydrolevoglucosenone (DLG or Cyrene®), and cyclic voltammetry studies of some organic molecules demonstrate its possible potential use in organic electrosynthesis as an alternative to the traditional polar aprotic solvents such as DMF, NMP, and DMAc. These last solvents are harmful and toxic; some of them are being phased out of industrial processes.
2. The conductivity behaviour, chronoamperometry, and cyclic voltammetry responses of DLG electrolytic solutions, as well as the electrochemical behaviour of representative organic molecules in this bio-renewable medium, provide useful information about the use of DLG as a solvent to achieve sustainable organic electro-transformations.
3. Future works will be directed to carry out electrosynthetic reactions using DLG as a green-solvent alternative. This not only offers a safer and non-toxic alternative to traditional organic solvents, but also gives relevant information about the electrolytic solutions that can be used in diverse fields, including electrochemistry.

Introduction

Organic electrochemistry has experienced significant development since the early 2000s,[1] proving to be an excellent technique for obtaining value-added materials from biomass,[2] advanced materials such as conducting polymers,[3] and highly reactive intermediates that can be used in designing new strategies for constructing new chemical bonds, and accessing complex molecules.[4–6] This technique aligns with at least 9 of the 12 principles of green chemistry, rendering it an environmentally friendly methodology.[7,8] However, one of the biggest concerns regarding this methodology is the use of aprotic organic solvents such as *N*,*N*-dimethylformamide (DMF), *N*,*N*-dimethylacetamide (DMAc) and *N*-methylpirrolidinone (NMP), which are classified as "substances of very high concern and

[a]*Instituto de Química, Universidad Nacional Autónoma de México, Circuito Exterior, Ciudad Universitaria, 04510 Ciudad de México, Mexico. E-mail: bafrontu@unam.mx*
[b]*Centro Conjunto de Investigación en Química Sustentable UAEM-UNAM, Toluca, 50200 Estado de México, Mexico*
[c]*Depto. Ing. Y C. Químicas, Universidad Iberoamericana, Prol. Reforma 880, 01219, Mexico*

risk handling".[9,10] Solvent selection guides and diverse articles have addressed their toxicity, environmental impact, and safety concerns, encouraging the search for more sustainable solvents.[11] Ideally, water could resolve this concern, but the solubility of organic compounds[12] limits its use as a solvent. Water/organic mixtures are generally used[13] to overcome this issue, although some organic compounds or reactive intermediates are incompatible with water. Therefore, the search for alternative sustainable solvents in organic electrochemistry is currently an active field of research.[14] Several solvents have emerged as greener alternatives in organic chemistry and are commercially available: 2-methyl-tetrahydrofurane (2-MeTHF),[15] propylene carbonate (PC),[16,17] Polarclean™, dimethylisosorbide[18] and dihydrolevoglucosenone (DLG or Cyrene™).[19] DLG is a dipolar aprotic solvent, bio-degradable, bio-renewable and non-toxic, manufactured on a large scale from cellulose biomass (Scheme 1).

According to Table 1, DLG possesses physicochemical properties similar to those of DMF, DMA, and NMP, including boiling point, polarity, and dielectric constant. Owing to these characteristics, it has been examined as an alternative solvent in organic reactions such as C–C cross-coupling reactions,[20–22] the synthesis of ureas[23] and amides,[24,25] among others, which evidences its potential as a green solvent alternative in organic chemistry. DLG's physicochemical features facilitate the solubility of common supporting electrolytes, positioning it as a potential candidate for green electrolytic solvents, instead of the traditionally used ones in organic electrochemistry. In a previous short report, the specific conductance behaviour of tetrabutylammonium salts as a supporting electrolyte in pure DLG and the first use of DLG as a solvent in organic electrosynthesis (benzophenone derivatives reduction) demonstrated its potential to successfully replace DMF.[31] In this paper the properties, molar conductivity, viscosity behaviour at different temperatures and IR spectroscopy studies of DLG tetraalkylammonium salts (Bu_4NBF_4, Bu_4NPF_6, Bu_4NClO_4) solutions were studied in detail. Furthermore, the electrochemical potential window of the prepared solutions was determined, and the electrochemical behaviour of representative electroactive compounds (ferrocene, phenol, EDOT, morpholine, indole, phthalimide and nitro derivatives) on this medium demonstrated the potential use of this green solvent in analytical and synthetic organic electrochemistry.

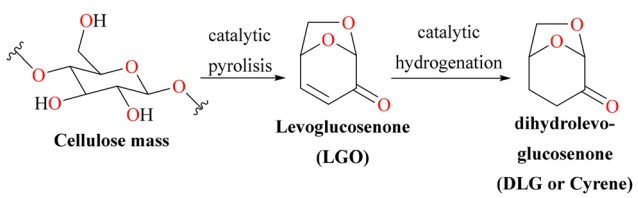

Scheme 1 Chemical obtention of DLG from cellulose mass.

Table 1 Physicochemical properties of traditional dipolar aprotic solvents and green dipolar solvents

Property	DLG	PC	NMP	DMF	DMA	DMSO
Bp (°C)	203[26]	242[27]	202[26]	153[28]	165[27]	189[26]
Density (g mL^{-1})	1.25[26]	1.20[29]	1.03[26]	0.948[28]	0.94[28]	1.10[26]
π^*	0.93[26]	0.83[30]	0.90[26]	0.88[28]	0.85[28]	1[26]
ε	37.3[27]	64.9[29]	33[27]	36.7[27]	37.8[27]	46.7[27]
Viscosity (cP)	14.5 (20 °C)[27]	2.52[29]	1.65[28]	0.92[27]	0.92[28]	1.99[27]

Results and discussion

In organic electrochemistry, the most commonly used electrolytic solutions contain tetraalkylammonium salts, such as Bu_4NBF_4, Bu_4NPF_6, and Bu_4NClO_4, in combination with dipolar aprotic solvents, including acetonitrile (ACN), dimethylformamide (DMF), *N*-methyl-2-pyrrolidone (NMP), and dimethylacetamide (DMAc). To explore the potential of replacing traditional solvents with greener alternatives, such as DLG, it is essential to understand the physicochemical properties of the electrolyte solutions. Therefore, the molar conductivity behaviour of Bu_4NBF_4, Bu_4NPF_6, Bu_4NClO_4, Et_4NBF_4, Et_4NPF_6, and $MeEt_3NBF_4$ solutions in freshly purified DLG (see SI) was analysed using the chemical model of conductivity based on the Lee and Wheaton equation in the Pethybridge and Taba suggested form (LWPT)[32] (see SI).

An inspection of Fig. 1 and Table 2 reveals that the molar conductivities of tetrabutylammonium salts are similar among themselves, with minor differences in the values obtained when the anion is changed, following the order Bu_4NBF_4 > Bu_4NClO_4 > Bu_4NPF_6. This same trend is observed in tetraethylammonium salts, where the order is Et_4NBF_4 > Et_4NPF_6. The most significant differences in conductivity values arise from varying the cations, following the order $MeEt_3N^+$ > Et_3N^+ > Bu_4N^+. As anticipated, the trend in Λ° values can be corrobo-

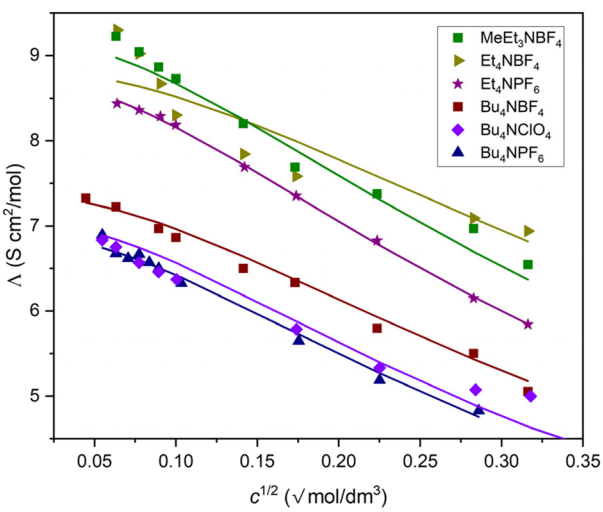

Fig. 1 Molar conductivity value of tetrabutylammonium salts *vs.* square root of the concentration in DLG at 298.15 K in the range of 0.002 M 0.2 M; symbols denote the experimental data, lines denote the LWPT calculations.

Table 2 Limiting molar conductivity ($\Lambda°$), the association constant (K_A), and Walden product ($\Lambda°\eta$) of tetraalkylammonium salts in DLG at T = 298.15 K

Supporting electrolyte	$\Lambda°$(S cm^2 mol^{-1}) (σ)	K_A	$\Lambda°\eta$ (S cm^2 mol^{-1} mPa s)
Bu_4NBF_4	7.36 (±0.36)	6.00	99.3
Bu_4NPF_6	6.90 (±0.22)	8.00	93.1
Bu_4NClO_4	7.05 (±0.56)	7.90	96.9
Et_4NBF_4	8.88 (±0.79)	3.83	119.8
Et_4NPF_6	8.72 (±0.07)	7.34	117.7
$MeEt_3NBF_4$	9.20 (±0.50)	6.43	124.2

rated by the Walden product $\Lambda°\eta$ (the product of limiting molar conductance and viscosity), where the higher values obtained for tetraethylammonium salts and $MeEt_3NBF_4$ reflect greater ion–solvent interaction than tetrabutylammonium salts; therefore, the latter exhibit a stronger ion-association.

To gain further insight into this point, the association constant (K_A) values obtained for the salts in DLG show an increase from Bu_4NBF_4 to Bu_4NPF_6, and a decrease from Bu_4NBF_4 to $MeEt_3NBF_4$. This behaviour illustrates the influence of the ions (cations and anions) in the solvation process in DLG. This observation can be rationalised by noting that the hexafluorophosphate anion possesses the largest ionic radius, which decreases solubility and favours ionic pair association. Thus, reducing the ionic radius of alkylammonium salts enhances solvation and increases conductivity. The molar conductivities in DLG are lower than those observed in dipolar aprotic solvents due to its high viscosity (*vide infra*), with a value of 13.5 cP for DLG compared to 0.9 for DMF (Table 1).

The limiting ionic conductivity ($\Lambda°$) of supporting electrolytes can be calculated by dividing $\Lambda°$ into its ionic components ($\lambda^{o\pm}$) according to Kohlrausch's law. However, without conductivity reported data for supporting electrolytes in DLG, we have utilised the reference electrolyte method[34] to separate $\Lambda°$ into its ionic components. In this instance, tetrabutylammonium tetraphenylborate (Bu_4NBPh_4) was employed as the reference electrolyte because the ionic radii values of the tetrabutylammonium cation and the tetraphenylborate anion are considered equal, and they have been used to evaluate the limiting ionic conductivities in several organic solvents.[29] Based on the limiting molar conductivity of Bu_4NBPh_4 ($\Lambda°$ = 6.7856 S cm^2 mol^{-1}) in DLG (see SI Fig. S1), the ionic contributions for Bu_4N^+ λ^{o+} = 3.3928 S cm^2 mol^{-1} and BPh_4^- λ^{o-} = 3.3928 S cm^2 mol^{-1} were calculated. Additionally, by applying the second law of Kohlrausch with these values, the limiting ionic conductance of other anions was determined (Table 3).

As we can see in Table 3, the $\lambda°$ follows the order: BF_4^- > ClO_4^- > PF_6^-, indicating that this value decreases with the increase of the ionic radii of the anions (BF_4^- = 2.27 Å, ClO_4^- = 2.36 Å, PF_6^- = 2.54 Å), even as the solubility of supporting electrolytes diminishes. For instance, the solubility of Bu_4NPF_6 in DLG reaches a maximum concentration of approximately 0.8 M. Additionally, as shown in Fig. 1, the $\Lambda°$ of supporting

Table 3 Limiting ionic conductance ($\lambda^{o\pm}$), ionic Walden product ($\lambda^{o\pm}\eta$), Stokes radii (r_s), dielectric friction coefficient (r_c), and diffusion coefficient (D_λ) of tetraalkylammonium salts in DLG at T = 298.15 K

Ion	$\lambda^{o\pm}$ (S cm^2 mol^{-1})	$\lambda^{o\pm}\eta$	r_s (Å)	r_c(Å)	D_λ (cm^2 s^{-1})
BF_4^-	3.967	53.5572	2.29	2.27[33]	1.056×10^{-6}
ClO_4^-	3.787	51.1272	2.40	2.36[33]	1.008×10^{-6}
PF_6^-	3.507	47.3472	2.59	2.54[33]	9.33×10^{-7}
Bu_4N^+	3.392	45.8028	2.68	4.11[33]	9.04×10^{-7}
Et_4N^+	4.912	66.3228	1.67	3.36[33]	1.30×10^{-6}
$MeEt_3N^+$	5.23	70.64	1.56	3.27[33]	1.39×10^{-6}

electrolytes increase with the smallest carbon chain, such as the Et_4N^+ cation, reaching values around 8.88–8.72 S cm^2 mol^{-1}, due to its smaller ionic radius (Et_4N^+ = 3.36 Å) compared to Bu_4N^+ (4.11 Å). Therefore, the ionic limit conductance of Et_4N^+ increases, and the same trend with anions is observed as in tetrabutylammonium salts. The Walden product ($\lambda^{o\pm}\eta$) indicates the interactions between the ions and the solvent (Table 3), and it is noted that it decreases from the methyltetraethylammonium to the tetrabutylammonium ion. This suggests that the electrostatic ion–solvent interactions are weak, likely due to the low surface charge density of the tetrabutylammonium ion compared with that of the methyltriethylammonium or tetraethylammonium ion, indicating that the surface charge densities of these ions level off with an increase in size. The calculation of hydrodynamic radii or Stokes' radii (r_s) was performed from the $\lambda^{o\pm}$ values according to the following expression (eqn (1)):[35]

$$r_s = \frac{|z_i|eF}{4\pi\eta\lambda^{o\pm}} \quad (1)$$

where z_i is the ion charge, e the electron charge, F the Faraday constant (C mol^{-1}), η the viscosity of the solvent (Pa s) and $\lambda^{o\pm}$ the limiting molar conductivity of the ion (S m^2 mol^{-1}). As shown in Table 3, the Stokes radii calculated for the anions BF_4^-, PF_6^-, ClO_4^-, are similar to their crystallographic radius, however, lower values are obtained for the quaternary ammonium ions. This suggests a limitation of the traditional Stokes' law model, which assumes a solid sphere in the presence of a solvent. Consequently, a revised version of Stokes' law was essential for acquiring data on quaternary ammonium cations.[36,37] Consequently, the diffusion coefficient value (D_λ) of all ions considered was obtained from limiting molar conductivity by using the following relation (eqn (2)):[38]

$$D_\lambda = \frac{kT}{e|z_i|F}\lambda_i^\circ \quad (2)$$

where k is the Boltzmann constant, and the other symbols have the same meanings as in eqn (1). The values obtained are summarised in Table 3. As expected, smaller molecules have higher diffusion coefficients for ions of the same charge. For tetraalkylammonium cations, their diffusion coefficient increases in the following order $MeEt_3N^+$ > Et_4N^+ > Bu_4N^+, as the carbon chain length decreases. This is due to the larger ionic radius of the longer carbon chains, which increases fric-

tion with the solvent than shorter carbon chains. However, owing to the high viscosity of DLG, the diffusion coefficient values of ions are at least one order of magnitude lower than those reported in DMF or acetonitrile.

The specific conductivity behaviour of the supporting electrolytes dissolved in Cyrene was studied as a function of temperature, ranging from 0 °C to 70 °C. DLG is a solvent with low vapour pressure; this property allows for heating without solvent loss due to evaporation, ensuring that the concentration of the supporting electrolyte remains constant during the study. As shown in Fig. 2, all studied supporting electrolytes exhibit linear behaviour. As the temperature increases, Bu_4NClO_4 becomes more conductive than Bu_4NPF_6; this can be attributed to the fact that the anion ClO_4^- has a smaller ionic radius than the anion PF_6^-, which facilitates better solvation by Cyrene. Although the ionic radii of ClO_4^- and BF_4^- are very similar, the ion–solvent interactions between Cyrene and BF_4^- promote better conductivity for the electrolyte solution compared to the DLG-ClO_4^- solvent-ion interaction. Furthermore, the heating of DLG enhances the decay of viscosity (*vide infra*), thereby increasing the conductivity of the solutions.

Viscosity behaviour of pure DLG and electrolyte solutions

For electrochemical applications, viscosity is a fundamental parameter to control because mass transfer processes, such as diffusion, govern the reaction kinetics. Therefore, acquiring information about the viscosity behaviour as a function of temperature for pure DLG and the electrolyte solutions is important. As shown in Fig. 3, at −10 °C, the viscosity of DLG reaches a value of 62 cP. As the temperature increases to 0 °C, the viscosity reduces to half of its initial value. Beyond this temperature, the viscosity decreases exponentially until it reaches 7.5 cP at 65 °C.

This behaviour suggests that DLG viscosity resembles that of ionic liquids.[39] Thus, the Vogel–Tammann–Fulcher (VTF) equation (eqn (3))[40–42] was used to characterise DLG's viscosity behaviour.

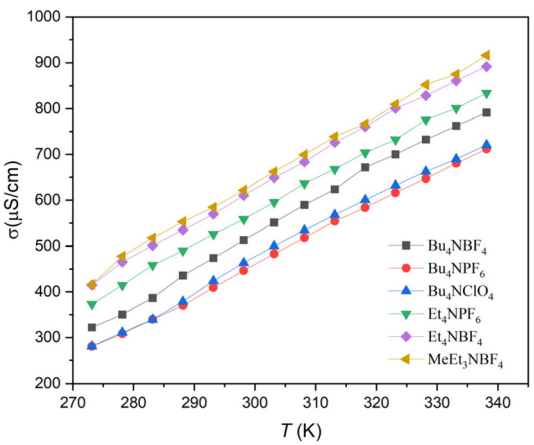

Fig. 2 Temperature dependence of molar conductivity of tetrabutylammonium salts in DLG from 273.15 K to 338.15 K.

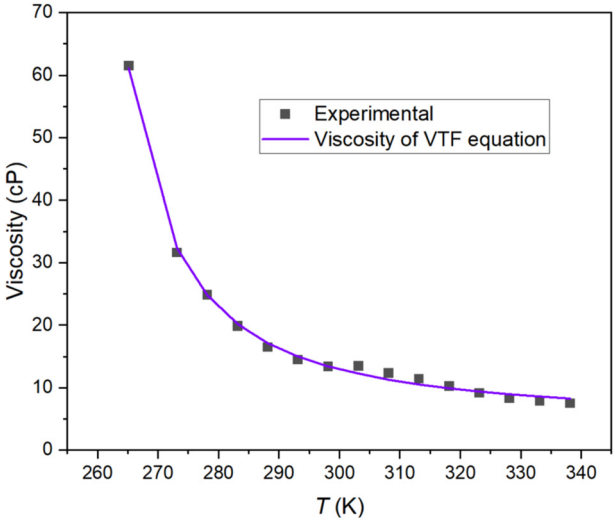

Fig. 3 Viscosity behaviour of DLG as a function of the temperature from 263.15 to 338.15 K. Symbols denote the experimental data and lines denote the VTF calculations.

$$\eta_0(T) = \eta_\infty \exp\left(\frac{B}{T - T_0}\right) \quad \text{or} \quad \ln \eta_0(T) = \ln \eta_\infty + \frac{B}{T - T_0} \quad (3)$$

The plot produced by the VTF equation aligns closely with the experimental data (Fig. 3) (see Fig. S2). Only minor deviations are noted when comparing the experimental data with the VTF equation, which can be attributed to internal molecular rearrangements that occur during the heating process due to changes in intermolecular hydrogen bonding interactions.

When supporting electrolytes are added to DLG at 25 °C using diluted concentration values (c < 0.5 M), they do not substantially alter the viscosity of pure DLG (13.5 cP), as illustrated in Fig. 4, remaining within the range of 13.5–15 cP.

For the quaternary salt Bu_4NBF_4, the viscosity begins to increase slightly from c = 0.008 M. When the concentration is raised to 0.4 M, the viscosity of the electrolytic solution reaches a value of 15 cP (red line dots). In the case of Bu_4NPF_6, a similar effect is observed; the viscosity of the electrolyte starts to increase slightly at c = 0.1 M, and with c = 0.2 M the viscosity reaches a value of 13.9 cP. The quaternary salt Bu_4NBF_4 renders the solution slightly more viscous than Bu_4NPF_6. This suggests that the anion BF_4^- appears to have more ion–solvent interactions with DLG than the PF_6^- anion. The viscosity behaviour of the electrolytic solutions of quaternary salts Bu_4NBF_4 and Bu_4NPF_6, both at a concentration of 0.15 M, was plotted as a function of temperature in comparison with pure DLG from 20 °C to 65 °C (Fig. 5). It can be observed that the Bu_4NBF_4 solution in DLG is slightly more viscous than pure DLG, but the deviations at these concentrations are within the range of ±0.5 cP.

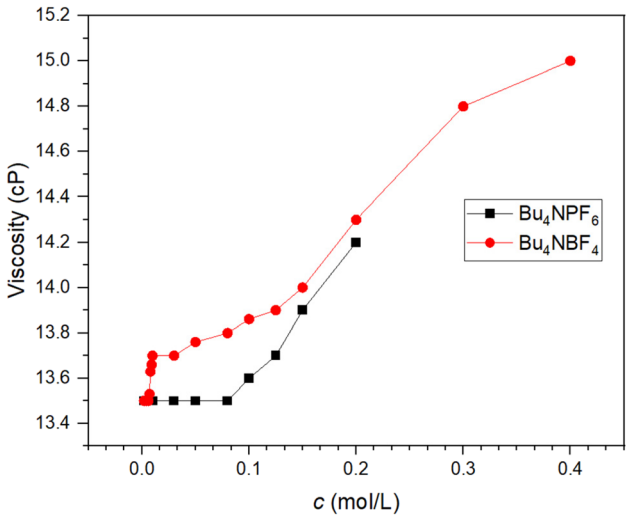

Fig. 4 Viscosity behaviour as a function of the concentration of supporting electrolytes at 298.15 K.

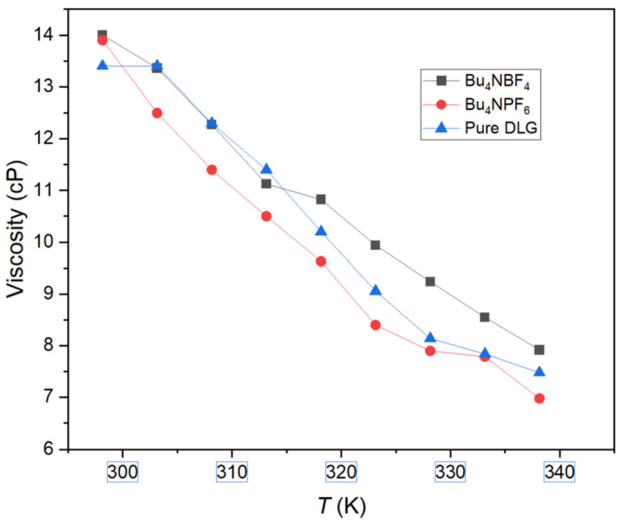

Fig. 5 Viscosity behaviour solution of 0.15 M of supporting electrolytes in DLG as a function of the temperature.

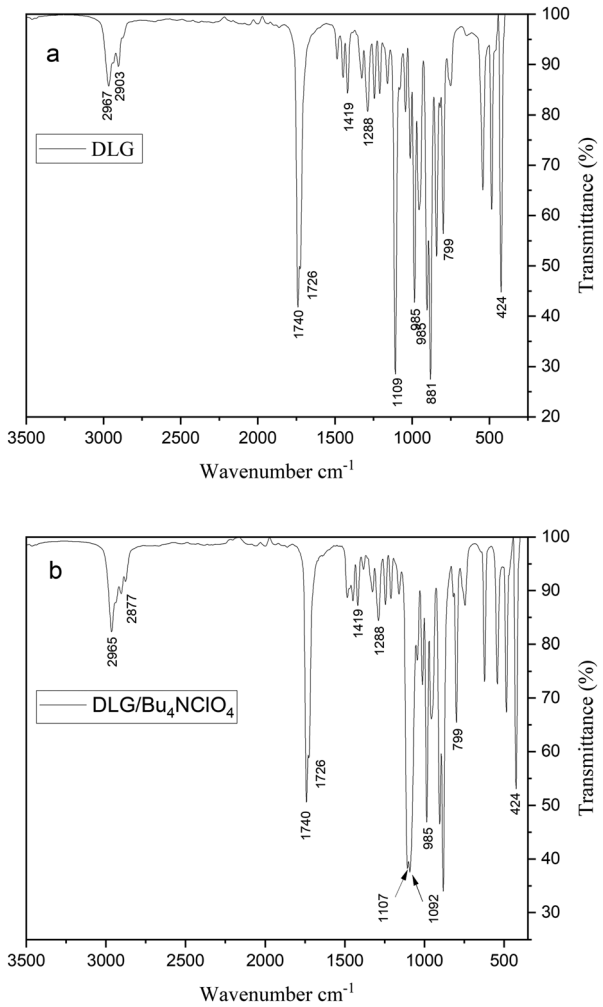

Fig. 6 IR (ATR) spectrumof (a) pure DLG and (b) spectrum of Bu_4NClO_4 1 M solutions in DLG.

ATR-FT-IR spectroscopic study of DLG electrolytes

It is well established that IR spectroscopic studies can be employed to investigate the solvation of supporting electrolytes in an organic medium.[43] For this reason, a series of IR spectroscopic studies were conducted to gain more information about the interactions of ammonium salts in DLG, which favours the solvation process. The chemical structure of DLG (Scheme 1) contains an internal cyclic ketal adjacent to the carbonyl group that provides a dipole moment of 4.40 D,[44] allowing interaction with cationic species either through the cyclic ketal or the carbonyl group. As expected, the IR spectrum of pure DLG show two absorption bands at 1740 cm^{-1} and 1726 cm^{-1} (Fig. 6) corresponding to the values reported in the literature. This phenomenon is attributed to the double absorption band of DLG, arising from the interaction of two DLG molecules that are very close to each other. The IR experimental spectrum under dilute conditions in CCl_4, the gas phase, and simulated results confirm this hypothesis by showing a single absorption band.[45] Also, the change in the position of the internal ketal in the case of iso-DLG[44] is reported, showing only one absorption band of the carbonyl group at 1733 cm^{-1}. Therefore, it is proposed that the C–H bond of the internal DLG ketal promotes structural aggregation through hydrogen bonding. Keeping in mind this aggregation phenomenon of DLG, we expected that the addition of supporting electrolyte would promote the breakup of the aggregation structure of DLG by solvating the supporting electrolyte, anticipating one absorption band of the carbonyl or a shift in the wavenumber due to the interaction of R_4N^+ cations with the carbonyl group, like DMF.[46] Despite this, as shown in the IR spectrum of Bu_4NBF_4 solution up to 1 M, the two absorption bands of the carbonyl group remain intact without any shift or change in the intensity of the absorption bands. This fact implies that the inter-

action of the carbonyl group with the R_4N^+ cations is slight or non-existent (Fig. 6).

Instead, the absorption band at 1109 cm^{-1}, corresponding to the C–O–C of the internal ketal, splits into two absorption bands, 1107 cm^{-1} and 1092 cm^{-1}; therefore, it is inferred that the interaction of R_4N^+ cations with DLG occurs through its internal ketal. Additionally, the absorption bands at 2967 cm^{-1} and 2903 cm^{-1}, corresponding to the C–H bond of the ketal, are affected by the presence of R_4N^+ cations, resulting in an increase in intensity and a shift to 2965 cm^{-1}, along with an increase in the intensity of the absorption band at 2877 cm^{-1}. Thus, these results suggest that the solvation of tetra-alkylammonium salts arises from the interaction of the internal cyclic ketal, rather than an interaction with the carbonyl group (see Fig. S3). The unaffected absorption bands of the carbonyl group in DLG suggest that hydrogen bonds between DLG molecules could also be stronger between the C–H bond of the ketal and the oxygen atoms of the ketal from another DLG molecule, instead of the participation of the carbonyl group, promoting structural aggregations. However, further studies are required to verify this hypothesis, which lies beyond the scope of this study.

Electrochemical behaviour of Ferrocene and *D* value in DLG

Cyclic voltammetry of ferrocene in this medium, utilising 0.15 M Bu_4NBF_4 and a glassy carbon electrode, was carried out (Fig. 7a), showing a reversible electrochemical system at $E_{1/2}$ = 0.136 V. The difference between the oxidation and reduction potential peaks is 73 mV, with a cathodic and anodic current ratio of I_{cp}/I_{ap} = 0.96 (Ru compensated 90%). The main disadvantage of DLG is its high viscosity (14.5 cP), which is approximately ten times higher than that of common dipolar aprotic solvents. This provokes a high ionic resistance in the solution and necessitates the use of a greater amount of supporting electrolyte (minimum 0.15 M). This viscosity problem can be overcome with the use of a co-solvent, for instance, the DLG blend with gamma-valerolactone (GVL) or 2-MeTHF (50 wt%) offers viscosity values ranging from 1.44 to 10 cP.[25] Particularly, the last one is a mixture that is commercially available and possesses a 100% renewable carbon content. This is particularly important in electrosynthesis, where mass transfer can be a limiting factor for successful and rapid large-scale transformations. Besides obtaining accurate CV signals, it is also essential to compensate for the ohmic drop (Ru, see SI). The current plot *versus* the square root of the scan rate indicates that diffusion controls the electrochemical process (Fig. 7b). The signals were distorted at higher scan rates (υ > 5 V s^{-1}).

To understand the effect of DLG viscosity on the diffusion process, the Fc diffusion coefficient (D) was determined using chronoamperometry as a redox reversible model, where the resulting current–time (I–t) response is described by the Cottrell equation (eqn (4)):

$$I = \frac{FA\sqrt{D}}{\sqrt{\pi t}}(C)_{\text{bulk}} \quad (4)$$

where D is the diffusion coefficient, C is the bulk concentration of species A in the solution, F is the Faraday constant, and A is the electrode area (for a disk with radius r_e, the area $A = \pi r_e^2$). Current–time transients were recorded for up to 10 s,[47] resulting from a potential step from the open-circuit potential to 0.45 V *vs.* $Ag/AgNO_3$, using the various supporting electrolytes mentioned above (Fig. S4a). The diffusion coefficient values obtained were at least one order of magnitude lower than those reported in acetonitrile or *N*,*N*-dimethylformamide, and they were similar to or higher than the values reported in some ionic liquids or eutectic solvents (Table 4). The difference in D values arises from the ion–solvent interaction between anions and DLG. The use of tetrabutylammonium perchlorate salt provides an electrolyte solution where ferrocene has a higher diffusion coefficient compared to those with Bu_4NBF_4 and Bu_4NPF_6, the latter having the smallest diffusion coefficient. This diffusion coefficient is also affected by substi-

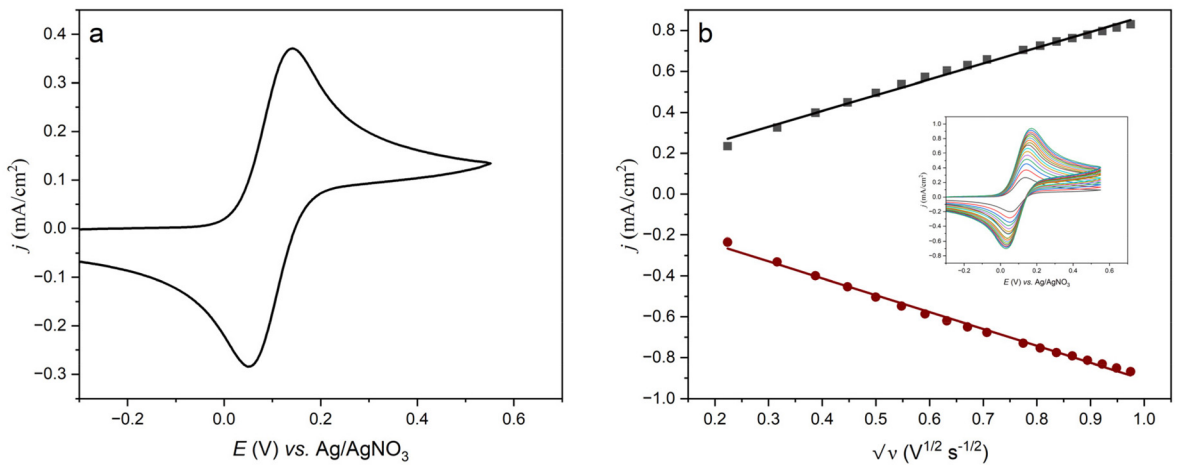

Fig. 7 (a) Cyclic voltammogram of ferrocene (5 mM) at a glassy carbon electrode in DLG (0.15 M of Bu_4NBF_4) at 298.15 K, Pt as a counter electrode, scan rate 0.1 V s^{-1}, Ru compensated 90% (b) plot of peak current *vs.* scan rate square root of the ferrocene in DLG at 298.15 K.

Table 4 Diffusion coefficients of ferrocene (5 mM) in DLG with different supporting electrolytes (0.15 M) at 298.15 K in comparison with other solvents

Solvent system	D (cm^2 s^{-1})
DLG/Bu_4NBF_4	9.06×10^{-7}
DLG/Bu_4NPF_6	6.11×10^{-7}
DLG/Bu_4NClO_4	1.076×10^{-6}
DLG/Et_4NBF_4	3.84×10^{-7}
DLG/Et_4NPF_6	5.84×10^{-7}
ACN[48]/(0.1 M) Bu_4NPF_6	2.24×10^{-5}
ACN[49]/(0.2 M) Bu_4NClO_4	2.2×10^{-5}
DMF[48]/(0.1 M) Bu_4NPF_6	0.95×10^{-5}
DMA[48]/(0.1 M) Bu_4NPF_6	0.76×10^{-5}
DMSO[48]/(0.1 M) Bu_4NPF_6	0.44×10^{-5}
DES: ethaline[50a]	9.0×10^{-8}
PC[51]/(0.1 M) $LiClO_4$	6.5×10^{-6}
$[(C_{n/2})_2Im][NTf_2]$[52] with n = 4,6,8,10	$1.8–6.5 \times 10^{-7}$

[a] Measured at 293.15 K

tuting the tetrabutylammonium salt with a smaller cation, such as tetraethylammonium salts, which yield slightly lower values.

These values were used to model the current behaviour using the Shoup–Szabo equation,[53] as depicted in Fig. S8b. The values obtained from the Cottrell equation appropriately fitted the previously presented CA data; the observed deviation from purely Cottrellian behaviour can be attributed to radial diffusion effects at the electrode.[54]

The behaviour of the ferrocene diffusion coefficient *versus* temperature was investigated from 25 °C (298.15 K) to 50 °C (323.15 K) with various supporting electrolytes, as shown in Fig. 8. Although the differences are minor, the D value in Bu_4NClO_4 is initially higher than for the other electrolytes. At a temperature of 303 K, the values of D are around 1×10^{-6} cm^2 s^{-1} and are quite similar among the different electrolyte compositions studied. As the temperature increases, the trend continues until 313.15 K, reaching values around 1.5×10^{-6} cm^2 s^{-1}. Subsequently, from 318.15 K, the ion–solvent interaction in DLG changes, and in the presence of Bu_4NPF_6, the diffusion coefficient increases more than in the other electrolytes. Following temperature increases, this trend is maintained for Bu_4NPF_6; however, for the electrolyte DLG-Bu_4NBF_4, the diffusion coefficient increases more than DLG-Bu_4NClO_4 electrolyte. This behaviour indicates that the solvent-anion interactions are modified as the temperature changes and are dependent on the anion of the Bu_4N^+ salt used.

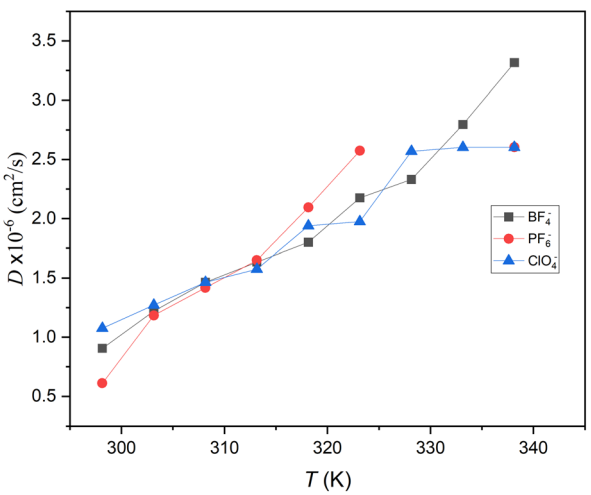

Fig. 8 Diffusion coefficient of ferrocene in different electrolytes in function of the temperature in DLG.

Heterogeneous electron-transfer rate constant (k°) of ferrocene in DLG

The heterogeneous electron transfer rate constant is a crucial parameter influenced by the electrode material, dynamic molecular solvent, and electrolyte composition. Ferrocene serves as the classical model, undergoing a rapid one-electron transfer process *via* outer-sphere electron transfer. With the electrochemical behaviour of ferrocene and its diffusion coefficient previously obtained, the k° of Fc in DLG at the glassy carbon electrode was evaluated using the Nicholson method.[55] Anodic and cathodic peak separations from a background were subtracted from a voltammogram of a simple one-electron transfer reaction and further utilised to determine ψ, from which k° was derived using eqn (5),

$$\psi = k\left(\frac{D_O n F \upsilon \pi}{RT}\right)^{\frac{1}{2}}\left(\frac{D_R}{D_O}\right)^{\frac{-\alpha}{2}} \quad (5)$$

where all other symbols have their usual meanings, for this experiment, the data were acquired at 298.15 K, C = 5 mM, and thus linear diffusion was expected to dominate; diffusion coefficients for both Fc and Fc$^+$ are considered equal. The charge transfer coefficient employed was α = 0.5. Under these conditions, the values of k° obtained for tetrabutylammonium/DLG electrolytes range from 3.3×10^{-3} to 4.8×10^{-3}. Similar k° values for Fc were also calculated using the equation reported by Magno.[56] The k° values determined are smaller than those for traditional polar aprotic solvents;[57,58] however, they are in the same order of magnitude or even higher than reported in ionic liquids[59–61] and deep eutectic solvents.[62] The main source of error in obtaining k° from Nicholson's method is the failure to achieve a correct compensation of the ohmic drop of the solution. To confirm the k° values obtained using this method, they were also determined from rotating disc electrode (RDE) experiments with Bu_4NBF_4/DLG electrolyte using Koutecky–Levich plots (Fig. 9). The corresponding I–E plots at different rotation velocities were obtained from linear voltammetry experiments (Fig. 9a), plotting the $1/I^{1/2}$ *vs.* $1/\omega^{1/2}$ (Fig. 9b) at different rotation velocities, ω, at different potentials of the Butler–Volmer region of the I–E plot, obtaining $1/I_k$. The k° value can be determined by plotting $\ln(I_k)$ against $(E–E^\circ)$, similar to Tafel plots, where the intercept value is equal to $nFAk^\circ C$, resulting in k° = 4.1 × 10^{-3} cm s^{-1}, which falls within the range obtained by Nicholson's method, thereby validating the results and confirming an adequate RU compensation methodology.

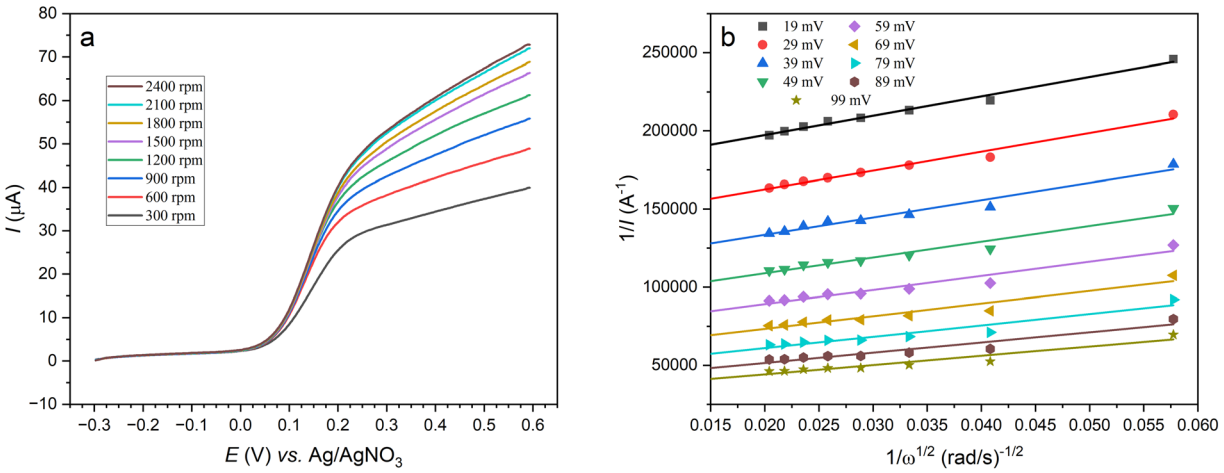

Fig. 9 (a) Rotating disk electrode (RDE) scans at different rotation rates and (b) Koutecky–Levich plots.

Electrochemical potential window of DLG and the redox behaviour of representative organic compounds

The electrochemical potential window of freshly purified DLG (see purification details in Fig. S6–S7 and Image S1–2) with different electrolytes was investigated using cyclic voltammetry on a glassy carbon electrode. As illustrated in the cyclic voltammogram in Fig. 10, when the Bu_4NBF_4 salt is employed, the anodic potential window of DLG reaches an exceptionally high value of 3.0 V, while the cathodic potential window attains a value of −2.2 V *vs.* $Ag/AgNO_3$. The first cycle was read out, and the cut-off current density for the electrochemical windows was taken at least 50 times the capacitive current density. A similar electrochemical window was observed with the BuN_4PF_6 and Bu_4NClO_4 salts; the replacement of tetrabutylammonium cation with Et_4N^+ and $MeEt_3N^+$ cations did not significantly affect the cathodic region either. With tetraalkylammonium cations and the BF_4^- anion, DLG exhibits a large potential window of 4.7 V. The comparison of the electrochemical potential window values with those reported in other solvents is depicted in Fig. 10b. DLG contains acidic protons (α-carbonyl), whereas ACN and DMF are considered aprotic solvents, which accounts for the narrower cathodic window observed.

These DLG potential windows were obtained using only clean and fresh purified DLG. When the direct commercial product or solvent was exposed to the environment for a couple of days, significant signals appeared in the CV (see SI), indicating that the solvent reacts with the environment, and the degradation products are electroactive. This reactivity is associated with the biodegradability of DLG, which makes it a non-toxic and environmentally friendly solvent; indeed, some fungi grew in a flask with DLG exposed for two weeks to the environment (see Fig. S11 SI). Consequently, once DLG was

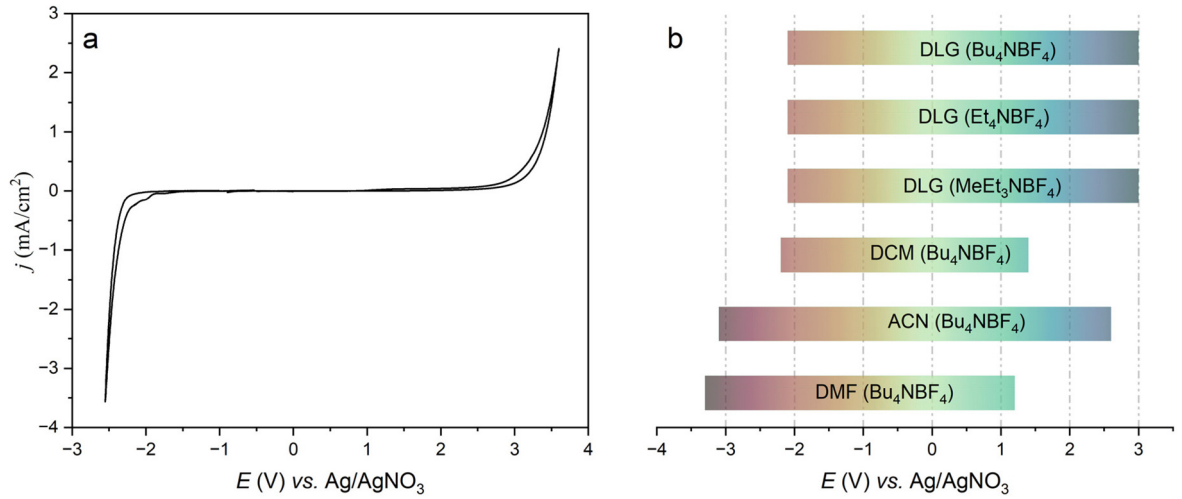

Fig. 10 (a) Cyclic voltammogram of DLG showing the electrochemical potential window. (b) Potential window of DLG electrolytes in comparison with dichloromethane, acetonitrile and DMF at glassy carbon electrode.

purified, it was maintained under an Ar or N_2 atmosphere without any deterioration signals or colour change for a month.

Fig. 11 illustrates the electrochemical behaviour of several representative organic compounds used in various applications. For instance, the oxidation of phenols under appropriate electrochemical conditions results in the formation of a wide array of reaction products including benzofurans,[63] dihydrobenzofurans,[64] and C–C and C–N dehydrogenative cross-coupling products.[65–68] In this regard, the electrochemical behaviour of 3,4-*tert*-butylhydroxyanisole (Fig. 11a) at a glassy carbon electrode in DLG presents an irreversible cyclic voltammogram featuring two distinctly defined oxidation peaks: the first peak at E = 0.87 V *vs.* Fc/Fc^+ and the second peak at E = 1.20 V *vs.* Fc/Fc^+, which shows an intriguing oxidation difference compared to other electrolyte conditions where the oxi-

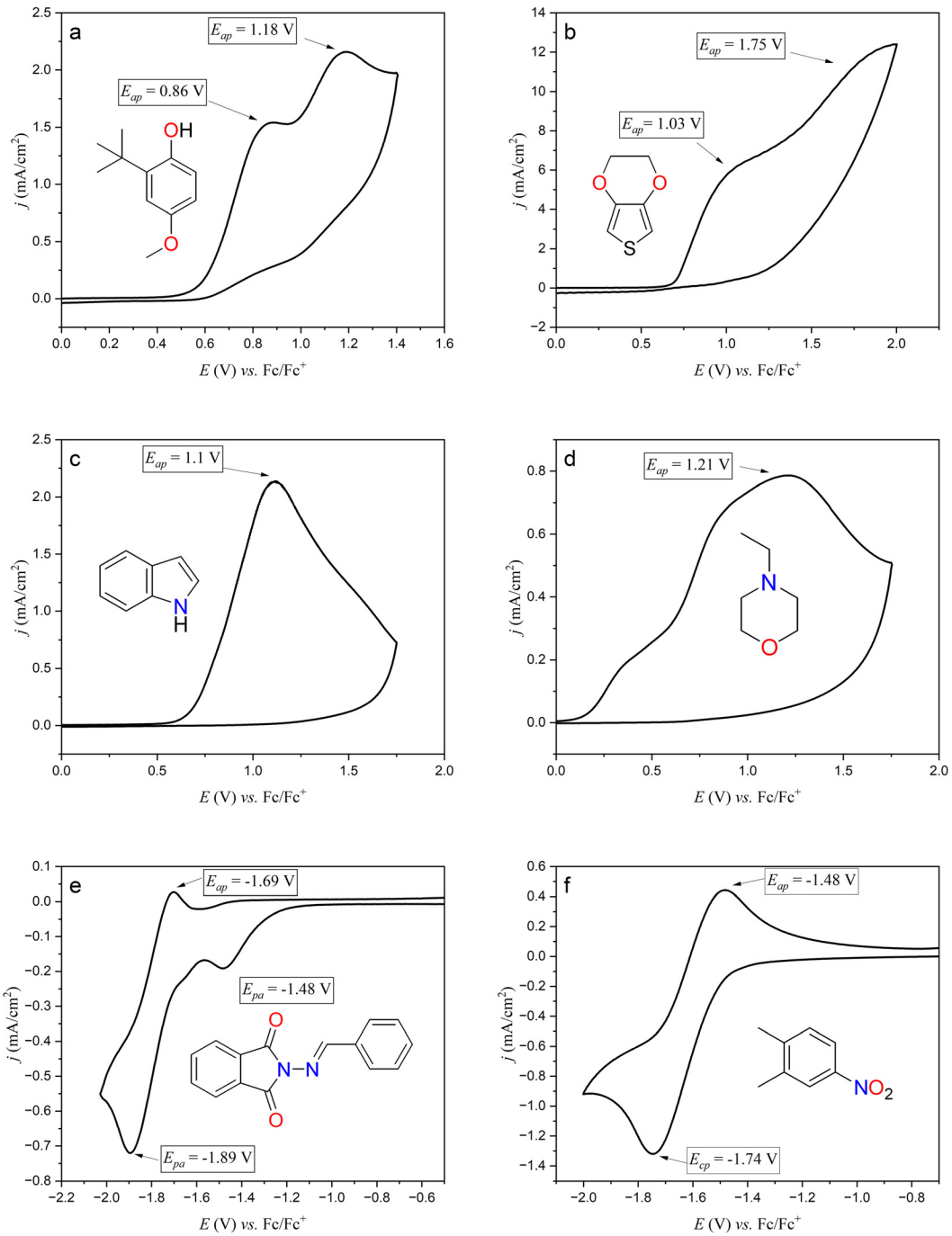

Fig. 11 Cyclic voltammograms of organic compounds (0.01 M) in DLG at glassy carbon electrode. (a) 3- *tert*-butyl-4-hydroxyanisole, (b) 3,4-ethylenedioxythiophene, (c) indole, (d) 4-ethylmorpholine, (e) *N*-(aminobenzyliden)-phthalimide, (f) 3,4-dimethylnitrobenzene.

dation of phenolic derivatives displays a single peak.[63] The electrochemical behaviour of the monomer 3,4-ethylendialkoxythiophene (EDOT, Fig. 11b) was analysed due to its polymeric form (PEDOT) obtained through electropolymerization, which has extensive applications in electrochemistry[69] and materials science.[70] The EDOT cyclic voltammogram exhibited the classical irreversible behaviour featuring two oxidation peaks: one at E = 1 V *vs.* Fc/Fc^+ and a second at E = 1.8 V *vs.* Fc/Fc^+. Additionally, an irreversible broad oxidation peak at E = 1.1 V *vs.* Fc/Fc^+ was observed for indole (Fig. 11c). This suggests that DLG could be used as a solvent for the anodic electropolymerization of these two monomers. As expected, the cyclic voltammogram of amine derivatives, such as 4-ethylmorpholine (Fig. 11d), used as a redox reagent in organic synthesis, reveals an irreversible form with a broad oxidation peak at E = 1.2 V *vs.* Fc/Fc^+.

Our exploration of various electroactive molecules on the cathodic side involved analysing *N*–*N*–imino-phthalimide (Fig. 11e), a potential mediator.[71] Its electrochemical response exhibits two reduction peaks: E = −1.48 V *vs.* Fc/Fc^+ (an irreversible pre-wave) and a quasi-reversible system centred at $E_{1/2}$ = −1.79 V *vs.* Fc/Fc^+, corresponding to the generation of the radical anion. Additionally, the cathodic reduction of nitrobenzene derivatives (Fig. 11f) was examined in this medium, revealing a quasi-reversible system centred at $E_{1/2}$ = −1.61 V *vs.* Fc/Fc^+, corresponding to the $Ar–NO_2^{\bullet-}$ radical anion system. The presence of quasi-reversible systems indicates the formation of stable radical anions in DLG, even though DLG is a potentially protic solvent. Consequently, this intriguing behaviour suggests that the protonation of these reactive species is very slow, thereby opening the possibility of using this biorenewable medium to conduct electro-reductions with electrogenerated radical anions on a preparative scale.[72–74] The electrochemical behaviour observed in DLG can be compared with the CV experiments carried out in common solvents such as acetonitrile (see Fig. S12), where differences in the electrochemical responses are observed for the majority of the molecules, indicating that the solvent can also modify the redox reactivity of the molecules. A short description of the main differences found between DLG and ACN behaviour can be found in the SI. No mechanistic studies were envisaged in this study to discuss these differences, and future studies will permit us to clarify this point. It is clear from this comparison that the electrochemical reaction in DLG could generate new reaction pathways that may become of great interest on a preparative scale.

Green score assessment of DLG as a solvent in electrosynthesis

Although DLG is considered a green solvent, it is essential to evaluate the greenness it offers, using green metrics. To assess the greenness of the electrosynthetic reaction using DLG as a solvent, the cathodic reduction of benzophenone carried out in DLG/EtOH mixture was selected and compared with the same electrochemical reaction performed in DMF.[31] The tool metric "Green Score" was employed for this purpose.[75] This tool metric is based on the 12 principles of green chemistry,[76] and these are grouped into five scoring categories: waste, sustainability, solvent, Health Safety and Environment (HSE), and Energy. For each category, specific questions based on CHEM21's,[77] and must be answered to obtain a global process assessment. Each answer is translated into several points and a corresponding colour (from 0 for red to 3 for green). The higher the overall mark, the greener the process. The methodology, the answers to those questions and the corresponding calculations are in SI. The comparative Green Score assessments for both reactions are shown in Fig. 12. Located at the centre of the snail-shaped diagram is the average of the item scores; similarly, the score for each item appears at the beginning of the circular graph. The electrochemical reaction performed in DLG has a value of 65, while the same process carried out in DMF has a value of 42. This indicates that the use of DLG in combination with EtOH provides a greener process. Analysing each item separated for both electrochemical processes, in the case of waste core, the parameters such as PMI (process mas intensity),[78] RME (reaction mass efficiency), stoichiometry and the yield are taken into account to this evaluation. The PMI values of the DLG/EtOH and DMF are 57.3 and 114.2, respectively. The lower the value, the less waste is generated, thereby increasing the score. From the sustainability perspective, the use of DLG as a renewable material

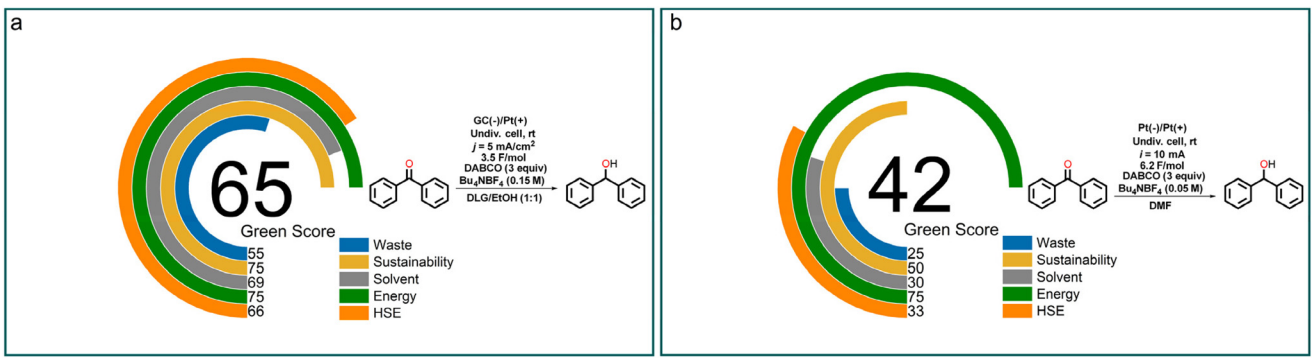

Fig. 12 (a) Green score assessment of the cathodic reduction of benzophenone carried out in DLG/EtOH mixture. (b) Comparison of the same reaction in DMF.

adds points over the score in comparison with the use of DMF, thereby increasing the greenness of the process. In the solvent score category, the overall rating ranges from 7 to 32, and the solvents are divided into four groups (green, yellow, orange and red). Each of these groups receives a score ranging from 0, for solvents to be avoided, to 3 for those recommended. DLG is ranked in the yellow group, obtaining a score of 69, while DMF is ranked in the red group with a score of 30, indicating it should be replaced. However, in this category, the solvents used for purifying the final product are taken into account, subtracting points from the score. Likewise, given the health, safety, and environmentally friendly features of DLG, it improves the score in the HSE category. Although the use of DABCO reduces the HSE scoring, resulting in a value of 66, the process with DMF as a solvent affords a low value of 33. The greenness score using DLG can be improved using water as a cosolvent. DLG is miscible with water, forming an equilibrium of carbonyl-geminal diol that enhances the solubility of certain organic compounds.[45] This blend opens the possibility of being used in future electrosynthetic reactions, but may be limited by its highly protic characteristic to only certain reactions.

Conclusions

The need to increase the green index of OES directs our attention towards exploring solvents regarded as promising replacements for traditional aprotic solvents. Due to the physicochemical properties of DLG, along with its degradability and natural origin, it emerges as a potential green solvent for OES. Given the environmental instability of DLG, we have briefly outlined its handling and purification before use in cyclic voltammetry to prevent impurity interference during electrochemical or electrosynthetic experiments. The molar conductivity behaviour of tetraalkylammonium salts in DLG showed that ion size affects this property. The ion–solvent interactions were investigated using IR spectroscopy, showing that the ketal function participates in solvation. Additionally, the information obtained regarding viscosity behaviour at varying temperatures enhanced our understanding, which may predict its potential applications in electrochemistry. The electrochemical aspects of ferrocene as a redox model molecule, including the diffusion coefficient, provide valuable insights into the influence of viscosity on mass transport within the electrochemical process, yielding values an order of magnitude lower, fitting within the range observed for ionic liquids and deep eutectic solvents. Similarly, the heterogeneous electron transfer value of ferrocene at glassy carbon in DLG aligns with the magnitudes reported for these latter solvents. A series of representative electroactive redox molecules were examined to confirm their potential for electrochemical transformation in this biomass-derived sustainable solvent for electroanalytical or electrosynthetic studies. Finally, its evaluation as a solvent in a described electrochemical transformation using the tool metric "Green Score" demonstrates its potential as a green solvent. Even if preparative scale transformations are beyond the scope of this work, the results obtained provide key information for designing electrochemical synthetic methodologies using DLG (Cyrene®) in the future.

Author contributions

J. M. Ramos Villaseñor and J. Sotelo-Gil conducted all experiments. M. P. Flores-Morales. J. M. Ramos Villaseñor wrote the original draft. R. Vasquéz-Medrano and B. A. Frontana-Uribe supervised the research. Revision and edition of the draft, conceptualisation and funding acquisition were done by B. A Frontana-Uribe.

Conflicts of interest

The authors declare that they have no known competing financial interests or personal relationships that could have appeared to influence the work reported in this paper.

Data availability

A key series of data is included in the SI: General experimental information, details on the conductivity and viscosity measurements, IR spectroscopy information, details about the measurement of diffusion coefficients, cyclic voltammetry data of ferrocene in DLG, impurities and purification of DLG, comparison of the studied organic compounds in ACN and DLG, green score assessment calculations for the electrochemical reduction of benzophenone. See DOI: **https://doi.org/10.1039/d5gc03356j**.

Other data that support the findings of this study are available at the shared file: **http://rdu.iquimica.unam.mx/handle/20.500.12214/1319**.

Acknowledgements

BAFU acknowledges the support of CONAHCYT project A1-S-18230 and the project PAPIIT-DGAPA UNAM IV 200222. JMRV thanks to CONAHCYT for the scholarship received (CVU-957122). We thank M. C. S. María Citlalit Martínez Soto, M. C. Alejandra Nuñez, M. C M. Nieves Zavala and M. C. Lizbeth Triana Cruz (CCIQS-UAEM-UNAM) for the technical support.

References

1 M. Yan, Y. Kawamata and P. S. Baran, *Chem. Rev.*, 2017, **117**, 13230–13319.
2 M. Zirbes and S. R. Waldvogel, *Curr. Opin. Green Sustainable Chem.*, 2018, **14**, 19–25.
3 T. Kurioka and S. Inagi, *Chem. Rec.*, 2021, **21**, 2107–2119.

4 E. J. Horn, B. R. Rosen and P. S. Baran, *ACS Cent. Sci.*, 2016, **2**, 302–308.
5 D. F. Chicas-Baños and B. A. Frontana-Uribe, *Chem. Rec.*, 2021, **21**, 2538–2573.
6 A. Shatskiy, H. Lundberg and M. D. Kärkäs, *ChemElectroChem*, 2019, **6**, 4067–4092.
7 B. A. Frontana-Uribe, R. D. Little, J. G. Ibanez, A. Palma and R. Vasquez-Medrano, *Green Chem.*, 2010, **12**, 2099.
8 S. Cembellín and B. Batanero, *Chem. Rec.*, 2021, **21**, 2453–2471.
9 F. Gao, R. Bai, F. Ferlin, L. Vaccaro, M. Li and Y. Gu, *Green Chem.*, 2020, **22**, 6240–6257.
10 A. Jordan, C. G. J. Hall, L. R. Thorp and H. F. Sneddon, *Chem. Rev.*, 2022, **122**, 6749–6794.
11 R. K. Henderson, C. Jiménez-González, D. J. C. Constable, S. R. Alston, G. G. A. Inglis, G. Fisher, J. Sherwood, S. P. Binks and A. D. Curzons, *Green Chem.*, 2011, **13**, 854.
12 F. Harnisch and U. Schröder, *ChemElectroChem*, 2019, **6**, 4126–4133.
13 M. Li and X. Cheng, *Isr. J. Chem.*, 2024, **64**, e202300067.
14 A. Prudlik, A. Matei, A. Scherkus, J. I. Bardagi, S. B. Beil and R. Francke, *Green Chem.*, 2025, **27**, 4280–4288.
15 A. Mouret, L. Leclercq, A. Mühlbauer and V. Nardello-Rataj, *Green Chem.*, 2014, **16**, 269–278.
16 J. S. Bello Forero, J. A. Hernández Muñoz, J. Jones Jr. and F. M. da Silva, *Curr. Org. Synth.*, 2016, **13**, 834–846.
17 J. Seidler, A. Roth, L. Vieira and S. R. Waldvogel, *ACS Sustainable Chem. Eng.*, 2023, **11**, 390–398.
18 A. Sarkar, R. May, Z. Valmonte and L. E. Marbella, *Energy Adv.*, 2022, **1**, 671–676.
19 J. E. Camp, *ChemSusChem*, 2018, **11**, 3048–3055.
20 S. Sangon, N. Supanchaiyamat, J. Sherwood, C. R. McElroy and A. J. Hunt, *React. Chem. Eng.*, 2020, **5**, 1798–1804.
21 K. Wilson, J. Murray, C. Jamieson and A. Watson, *Synlett*, 2018, 650–654.
22 N. A. Stini, P. L. Gkizis and C. G. Kokotos, *Green Chem.*, 2022, **24**, 6435–6449.
23 L. Mistry, K. Mapesa, T. W. Bousfield and J. E. Camp, *Green Chem.*, 2017, **19**, 2123–2128.
24 K. L. Wilson, J. Murray, C. Jamieson and A. J. B. Watson, *Org. Biomol. Chem.*, 2018, **16**, 2851–2854.
25 C. Sullivan, Y. Zhang, G. Xu, L. Christianson, F. Luengo, T. Halkoski and P. Gao, *Green Chem.*, 2022, **24**, 7184–7193.
26 J. Sherwood, M. De bruyn, A. Constantinou, L. Moity, C. R. McElroy, T. J. Farmer, T. Duncan, W. Raverty, A. J. Hunt and J. H. Clark, *Chem. Commun.*, 2014, **50**, 9650–9652.
27 D. Zhao, J. F. Kim, G. Ignacz, P. Pogany, Y. M. Lee and G. Szekely, *ACS Nano*, 2019, **13**, 125–133.
28 D. Kong and A. V. Dolzhenko, *Sustainable Chem. Pharm.*, 2022, **25**, 100591.
29 N. Peruzzi, P. Lo Nostro, B. W. Ninham and P. Baglioni, *J. Solution Chem.*, 2015, **44**, 1224–1239.
30 E. Andrzejewska, *Polym. Int.*, 2017, **66**, 366–381.
31 J. M. Ramos-Villaseñor, J. Sotelo-Gil, S. E. Rodil and B. A. Frontana-Uribe, *Faraday Discuss.*, 2023, **247**, 179–191.
32 S. S. Taba and A. D. Pethybridge, *J. Chem. Soc., Faraday Trans.*, 1980, **76**, 368–376.
33 J. F. Reardon, *Electrochim. Acta*, 1987, **32**, 1595–1600.
34 R. M. Fuoss and E. Hirsch, *J. Am. Chem. Soc.*, 1960, **82**, 1013–1017.
35 O. E. Zhuravlev, I. I. Lebedev and G. S. Yulmasov, *Russ. J. Phys. Chem.*, 2023, **97**, 1453–1458.
36 H. Sadek, *J. Electroanal. Chem. Interfacial Electrochem.*, 1983, **144**, 11–32.
37 Y. Marcus, *J. Solution Chem.*, 2012, **41**, 2082–2090.
38 M. Bešter-Rogač, M. V. Fedotova, S. E. Kruchinin and M. Klähn, *Phys. Chem. Chem. Phys.*, 2016, **18**, 28594–28605.
39 J. Safarov, G. Huseynova, M. Bashirov, E. Hassel and I. M. Abdulagatov, *Phys. Chem. Liq.*, 2018, **56**, 703–717.
40 H. Vogel, *Phys. Z.*, 1921, **22**, 645–646.
41 G. Tammann and W. Hesse, *Z. Anorg. Allg. Chem.*, 1926, **156**, 245–257.
42 G. S. Fulcher, *J. Am. Ceram. Soc.*, 1925, **8**, 339–355.
43 J. O. Bockris and A. K. N. Reddy, *Modern Electrochemistry 1: Ionics*, Kluwer Academic Publishers, Boston, MA, 2nd edn, 2002.
44 X. Liu, B. Pollard, M. G. Banwell, L.-J. Yu, M. L. Coote, M. G. Gardiner, B. M. A. Van Vugt-Lussenburg, B. Van Der Burg, F. L. Grasset, E. Campillo, J. Sherwood, F. P. Byrne and T. J. Farmer, *Aust. J. Chem.*, 2022, **75**, 331–344.
45 M. De bruyn, V. L. Budarin, A. Misefari, S. Shimizu, H. Fish, M. Cockett, A. J. Hunt, H. Hofstetter, B. M. Weckhuysen, J. H. Clark and D. J. Macquarrie, *ACS Sustainable Chem. Eng.*, 2019, **7**, 7878–7883.
46 I. Banik and M. N. Roy, *J. Chem. Eng. Data*, 2013, **58**, 3378–3386.
47 L. Xiong, L. Aldous, M. C. Henstridge and R. G. Compton, *Anal. Methods*, 2012, **4**, 371–376.
48 N. G. Tsierkezos, *J. Solution Chem.*, 2007, **36**, 289–302.
49 J. E. Baur and R. M. Wightman, *J. Electroanal. Chem. Interfacial Electrochem.*, 1991, **305**, 73–81.
50 S. Fryars, E. Limanton, F. Gauffre, L. Paquin, C. Lagrost and P. Hapiot, *J. Electroanal. Chem.*, 2018, **819**, 214–219.
51 J. Janisch, A. Ruff, B. Speiser, C. Wolff, J. Zigelli, S. Benthin, V. Feldmann and H. A. Mayer, *J. Solid State Electrochem.*, 2011, **15**, 2083–2094.
52 M. Thakurathi, E. Gurung, M. M. Cetin, V. D. Thalangamaarachchige, M. F. Mayer, C. Korzeniewski and E. L. Quitevis, *Electrochim. Acta*, 2018, **259**, 245–252.
53 D. Shoup and A. Szabo, *J. Electroanal. Chem. Interfacial Electrochem.*, 1982, **140**, 237–245.
54 K. Ngamchuea, S. Eloul, K. Tschulik and R. G. Compton, *J. Solid State Electrochem.*, 2014, **18**, 3251–3257.
55 R. S. Nicholson, *Anal. Chem.*, 1965, **37**, 1351–1355.
56 I. Lavagnini, R. Antiochia and F. Magno, *Electroanalysis*, 2004, **16**, 505–506.
57 N. G. Tsierkezos and U. Ritter, *J. Appl. Electrochem.*, 2010, **40**, 409–417.
58 R. Kaur, A. Ghoshal, P. Galav and P. C. Mondal, *Chem. – Asian J.*, 2024, **19**, e202400744.

59 N. Siraj, G. Grampp, S. Landgraf and K. Punyain, *Z. Phys. Chem.*, 2013, **227**, 105–120.
60 C. L. Bentley, J. Li, A. M. Bond and J. Zhang, *J. Phys. Chem. C*, 2016, **120**, 16516–16525.
61 Y. Pan, W. E. Cleland and C. L. Hussey, *J. Electrochem. Soc.*, 2012, **159**, F125–F133.
62 L. Bahadori, N. S. A. Manan, M. H. Chakrabarti, M. A. Hashim, F. S. Mjalli, I. M. AlNashef, M. A. Hussain and C. T. J. Low, *Phys. Chem. Chem. Phys.*, 2013, **15**, 1707–1714.
63 S. Lips, B. A. Frontana-Uribe, M. Dörr, D. Schollmeyer, R. Franke and S. R. Waldvogel, *Chem. – Eur. J.*, 2018, **24**, 6057–6061.
64 Q. Zhao, J.-K. Jin, J. Wang, F.-L. Zhang and Y.-F. Wang, *Chem. Sci.*, 2020, **11**, 3909–3913.
65 A. Kirste, B. Elsler, G. Schnakenburg and S. R. Waldvogel, *J. Am. Chem. Soc.*, 2012, **134**, 3571–3576.
66 B. Elsler, D. Schollmeyer, K. M. Dyballa, R. Franke and S. R. Waldvogel, *Angew. Chem., Int. Ed.*, 2014, **53**, 5210–5213.
67 K. Liu, S. Tang, P. Huang and A. Lei, *Nat. Commun.*, 2017, **8**, 775.
68 P. Feng, G. Ma, X. Chen, X. Wu, L. Lin, P. Liu and T. Chen, *Angew. Chem., Int. Ed.*, 2019, **58**, 8400–8404.
69 Y. Hui, C. Bian, S. Xia, J. Tong and J. Wang, *Anal. Chim. Acta*, 2018, **1022**, 1–19.
70 Z. Rahimzadeh, S. M. Naghib, Y. Zare and K. Y. Rhee, *J. Mater. Sci.*, 2020, **55**, 7575–7611.
71 E. S. Patiño-Alonzo, J. Barroso-Flores and B. A. Frontana-Uribe, *ChemCatChem*, 2023, **15**, e202300489.
72 A. Frontana-Uribe and C. Moinet, *Tetrahedron*, 1998, **54**, 3197–3206.
73 B. A. Frontana-Uribe, C. Moinet and L. Toupet, *Eur. J. Org. Chem.*, 1999, 419–430.
74 T. Wirtanen, E. Rodrigo and S. R. Waldvogel, *Adv. Synth. Catal.*, 2020, **362**, 2088–2101.
75 F. Pin, J. Picard and S. Dhulut, *Org. Process Res. Dev.*, 2025, **29**, 1715–1726.
76 H. C. Erythropel, J. B. Zimmerman, T. M. de Winter, L. Petitjean, F. Melnikov, C. H. Lam, A. W. Lounsbury, K. E. Mellor, N. Z. Janković, Q. Tu, L. N. Pincus, M. M. Falinski, W. Shi, P. Coish, D. L. Plata and P. T. Anastas, *Green Chem.*, 2018, **20**, 1929–1961.
77 C. R. McElroy, A. Constantinou, L. C. Jones, L. Summerton and J. H. Clark, *Green Chem.*, 2015, **17**, 3111–3121.
78 E. R. Monteith, P. Mampuys, L. Summerton, J. H. Clark, B. U. W. Maes and C. R. McElroy, *Green Chem.*, 2020, **22**, 123–135.